

Integrated chalcogenide waveguide resonators for mid-IR sensing: leveraging material properties to meet fabrication challenges

Nathan Carlie,¹ J. David Musgraves,^{1,*} Bogdan Zdyrko,¹ Igor Luzinov,¹ Juejun Hu,^{2,3}
Vivek Singh,² Anu Agarwal,² Lionel C. Kimerling,² Antonio Canciamilla,⁴
Francesco Morichetti,^{4,5} Andrea Melloni,⁴ and Kathleen Richardson¹

¹*School of Materials Science and Engineering, Center for Optical Materials Science and Engineering Technologies (COMSET), Clemson University, Clemson, South Carolina 29634, USA*

²*Microphotonics Center, Massachusetts Institute of Technology, Cambridge, Massachusetts 02139, USA*

³*Department of Materials Science & Engineering, University of Delaware, Newark, Delaware 19716, USA*

⁴*Dipartimento di Elettronica e Informazione, Politecnico di Milano, Milano, Italy*

⁵*Fondazione Politecnico di Milano, Milano, Italy*

*jdm047@clemson.edu

Abstract: In this paper, attributes of chalcogenide glass (ChG) based integrated devices are discussed in detail, including origins of optical loss and processing steps used to reduce their contributions to optical component performance. Specifically, efforts to reduce loss and tailor optical characteristics of planar devices utilizing solution-based glass processing and thermal reflow techniques are presented and their results quantified. Post-fabrication trimming techniques based on the intrinsic photosensitivity of the chalcogenide glass are exploited to compensate for fabrication imperfections of ring resonators. Process parameters and implications on enhancement of device fabrication flexibility are presented.

©2010 Optical Society of America

OCIS codes: (140.3948) Micro-cavity devices; (070.5753) Resonators; (130.3120) Integrated optics devices; (130.3060) Infrared; (130.6010) Sensors.

References and links

1. J. Hu, X. Sun, A. Agarwal, and L. C. Kimerling, "Design guidelines for optical resonator biochemical sensors," *J. Opt. Soc. Am. B* **26**(5), 1032–1041 (2009).
2. J. Hu, N. Carlie, L. Petit, A. Agarwal, K. Richardson, and L. C. Kimerling, "Cavity-enhanced infrared absorption in planar chalcogenide glass resonators: experiment & analysis," *J. Lightwave Technol.* **27**(23), 5240–5245 (2009).
3. J. Hu, "Ultra-sensitive chemical vapor detection using micro-cavity photothermal spectroscopy," *Opt. Express* **18**(21), 22174–22186 (2010).
4. J. Hu, V. Tarasov, N. Carlie, N. N. Feng, L. Petit, A. Agarwal, K. Richardson, and L. Kimerling, "Si-CMOS-compatible lift-off fabrication of low-loss planar chalcogenide waveguides," *Opt. Express* **15**(19), 11798–11807 (2007).
5. L. Petit, N. Carlie, F. Adamietz, M. Couzi, V. Rodriguez, and K. C. Richardson, "Correlation between physical, optical and structural properties of sulfide glasses in the system Ge-Sb-S," *Mater. Chem. Phys.* **97**(1), 64–70 (2006).
6. W. Li, S. Seal, C. Rivero, C. Lopez, K. Richardson, A. Pope, A. Schulte, S. Myneni, H. Jain, K. Antoine, and A. Miller, "Role of S/Se ratio in chemical bonding of As-S-Se glasses investigated by Raman, x-ray photoelectron, and extended x-ray absorption fine structure spectroscopies," *J. Appl. Phys.* **98**(5), 053503 (2005).
7. A. Wilhelm, C. Boussard-Plédel, Q. Coulombier, J. Lucas, B. Bureau, and P. Lucas, "Development of Far-Infrared-Transmitting Te Based Glasses Suitable for Carbon Dioxide Detection and Space Optics," *Adv. Mater. (Deerfield Beach Fla.)* **19**(22), 3796–3800 (2007).
8. J. Hu, M. Torregiani, F. Morichetti, N. Carlie, A. Agarwal, K. Richardson, L. C. Kimerling, and A. Melloni, "Resonant cavity-enhanced photosensitivity in As₂S₃ chalcogenide glass at 1550 nm telecommunication wavelength," *Opt. Lett.* **35**(6), 874–876 (2010).
9. J. Hu, X. Sun, A. M. Agarwal, J.-F. Viens, L. C. Kimerling, L. Petit, N. Carlie, K. C. Richardson, T. Anderson, J. Choi, and M. Richardson, "Studies on Structural, Electrical and Optical Properties of Cu-doped As-Se-Te Chalcogenide Glasses," *J. Appl. Phys.* **101**(6), 063520 (2007).
10. E. Mytilineou, "Chalcogenide amorphous semiconductors: chemical modification or doping?" *J. Optoelectron. Adv. Mater.* **4**, 705–710 (2002).

11. C. Moynihan, P. Macedo, M. Maklad, R. Mohr, and R. Howard, "Intrinsic and Impurity Infrared Absorption in As_2Se_3 Glass," *J. Non-Cryst. Solids* **17**(3), 369–385 (1975).
12. J. S. Sanghera, V. Q. Nguyen, P. C. Pureza, F. H. Kung, R. Miklos, and I. D. Aggarwal, "Fabrication of Low-Loss IR-Transmitting $\text{Ge}_{30}\text{As}_{10}\text{Se}_{30}\text{Te}_{30}$ Glass Fibers," *J. Lightwave Technol.* **12**(5), 737–741 (1994).
13. V. Shiryayev, S. Smetanin, D. Ovchinnikov, M. Churbanov, E. Kryukova, and V. Plotnichenko, "Effects of Oxygen and Carbon Impurities on the Optical Transmission of As_2Se_3 Glass," *Inorg. Mater.* **41**(3), 308–314 (2005).
14. J. Hu, V. Tarasov, A. Agarwal, L. Kimerling, N. Carlie, L. Petit, and K. Richardson, "Fabrication and testing of planar chalcogenide waveguide integrated microfluidic sensor," *Opt. Express* **15**(5), 2307–2314 (2007).
15. A. M. Reitter, A. N. Sreeram, A. K. Varshneya, and D. R. Swiler, "Modified preparation procedure for laboratory melting of multicomponent chalcogenide glasses," *J. Non-Cryst. Solids* **139**, 121–128 (1992).
16. W. A. King, A. G. Clare, and W. C. LaCourse, "Laboratory preparation of highly pure As_2Se_3 glass," *J. Non-Cryst. Solids* **181**(3), 231–237 (1995).
17. T. Barwicz, and H. Haus, "Three-dimensional analysis of scattering losses due to sidewall roughness in microphotonic waveguides," *J. Lightwave Technol.* **23**(9), 2719–2732 (2005).
18. H. Liu, Y. Lin, and W. Hsu, "Sidewall roughness control in advanced silicon etch process," *Microsyst. Technol.* **10**(1), 29–34 (2003).
19. M. Borselli, T. J. Johnson, and O. Painter, "Accurate measurement of scattering and absorption loss in microphotonic devices," *Opt. Lett.* **32**(20), 2954–2956 (2007).
20. D. Sparacin, R. Sun, A. Agarwal, M. Beals, J. Michel, L. C. Kimerling, T. Conway, A. Pomerene, D. Carothers, M. Grove, D. Gill, M. Rasras, S. Patel, and A. White, "Low-Loss Amorphous Silicon Channel Waveguides for Integrated Photonics," in *Proceedings of 3rd IEEE International Conference on Group IV Photonics*, pp. 255–257.
21. J. Hu, V. Singh, A. Agarwal, and L. C. Kimerling, "Separation of scattering and absorption loss contributions in high-index-contrast optical resonators," manuscript in preparation.
22. M. Webster, R. Pafchek, G. Sukumaran, and T. Koch, "Low-loss quasi-planar ridge waveguides formed on thin silicon-on-insulator," *Appl. Phys. Lett.* **87**(23), 231108 (2005).
23. Y. Ruan, W. Li, R. Jarvis, N. Madsen, A. Rode, and B. Luther-Davies, "Fabrication and characterization of low loss rib chalcogenide waveguides made by dry etching," *Opt. Express* **12**(21), 5140–5145 (2004).
24. D. Choi, S. Madden, A. Rode, R. Wang, and B. Luther-Davies, "Plasma etching of As_2S_3 films for optical waveguides," *J. Non-Cryst. Solids* **354**(27), 3179–3183 (2008).
25. A. Tverjanovich, "Calculation of viscosity of chalcogenide glasses near glass transition temperature from heat capacity or thermal expansion data," *J. Non-Cryst. Solids* **298**(2-3), 226–231 (2002).
26. S. Dutta, H. Jackson, and J. Boyd, "Reduction of scattering from a glass thin-film optical waveguide by CO_2 laser annealing," *Appl. Phys. Lett.* **37**(6), 512–514 (1980).
27. R. Syms, and A. Holmes, "Reflow and Burial of Channel Waveguides Formed in Sol-Gel Glass on Si Substrates," *IEEE Photon. Technol. Lett.* **5**(9), 1077–1079 (1993).
28. J. Hu, N. N. Feng, N. Carlie, L. Petit, A. Agarwal, K. Richardson, and L. C. Kimerling, "Optical loss reduction in high-index-contrast chalcogenide glass waveguides via thermal reflow," *Opt. Express* **18**(2), 1469–1478 (2010).
29. <http://www.amorphousmaterials.com/IR%20Fibers.htm>
30. R. Wang, S. Madden, C. Zha, A. Rode, and B. Luther-Davies, "Annealing induced phase transformation in amorphous As_2S_3 films," *J. Appl. Phys.* **100**(6), 063524 (2006).
31. We have experimentally observed second phase precipitates and optical loss increase in Ge-Sb-S glass waveguides and resonators reflowed at temperatures above 300 °C.
32. S. Song, N. Carlie, J. Boudies, L. Petit, K. Richardson, and C. B. Arnold, "Spin-Coating of $\text{Ge}_{23}\text{Sb}_7\text{S}_{70}$ Chalcogenide Glass Thin Films," *J. Non-Cryst. Solids* **355**(45-47), 2272–2278 (2009).
33. C. Tsay, E. Mujagić, C. K. Madsen, C. F. Gmachl, and C. B. Arnold, "Mid-infrared characterization of solution-processed As_2S_3 chalcogenide glass waveguides," *Opt. Express* **18**(15), 15523–15530 (2010).
34. A. Atkinson, J. Doorbar, A. Hudd, D. L. Segal, and P. J. White, "Continuous ink-jet printing using sol-gel "Ceramic" inks," *J. Sol-Gel Sci. Technol.* **8**(1-3), 1093–1097 (1997).
35. H. Nagata, S. W. Ko, E. Hong, C. A. Randall, S. Trolier-McKinstry, P. Pinceloup, D. Skamser, M. Randall, and A. Tajuddin, "Microcontact Printed BaTiO₃ and LaNiO₃ Thin Films for Capacitors," *J. Am. Ceram. Soc.* **89**, 2816–2821 (2006).
36. X. Yu, Z. Wang, and Y. Han, "Microlenses fabricated by discontinuous dewetting and soft lithography," *Microelectron. Eng.* **89**, 18781881 (2008).
37. K. Y. Suh, Y. S. Kim, and H. H. Lee, "Capillary Force Lithography," *Adv. Mater. (Deerfield Beach Fla.)* **13**(18), 1386–1389 (2001).
38. A. van Popta, R. Decorby, C. Haugen, T. Robinson, J. McMullin, D. Tonchev, and S. Kasap, "Photoinduced refractive index change in As_2Se_3 by 633nm illumination," *Opt. Express* **10**(15), 639–644 (2002).
39. G. Yang, H. Jain, A. Ganjoo, D. Zhao, Y. Xu, H. Zeng, and G. Chen, "A photo-stable chalcogenide glass," *Opt. Express* **16**(14), 10565–10571 (2008).
40. P. Lucas, "Energy landscape and photoinduced structural changes in chalcogenide glasses," *J. Phys. Condens. Matter* **18**(24), 5629–5638 (2006).
41. A. Zoubir, M. Richardson, C. Rivero, A. Schulte, C. Lopez, K. Richardson, N. Hô, and R. Vallée, "Direct femtosecond laser writing of waveguides in As_2S_3 thin films," *Opt. Lett.* **29**(7), 748–750 (2004).

42. O. Efimov, L. Glebov, K. Richardson, E. Van Stryland, T. Cardinal, S. Park, M. Couzi, and J. Bruneel, "Waveguide writing in chalcogenide glasses by a train of femtosecond laser pulses," *Opt. Mater.* **17**(3), 379–386 (2001).
43. S. Song, N. Carlie, L. Petit, K. Richardson, and C. B. Arnold, "Spin-Coated Ge₂₃Sb₇S₇₀ Thin Films with Large Photo-Induced Refractive Index Change" Conference on Lasers and Electro-Optics (CLEO): CTuG6 (2010).
44. J. J. Santiago, M. Sano, M. Hamman, and N. Chen, "Growth and optical characterization of spin-coated As₂S₃ multilayer thin films," *Thin Solid Films* **147**(3), 275–284 (1987).
45. S. Song, C. F. Gmachl, and C. B. Arnold, "Solvent-casting of Photo-refractive Chalcogenide Glasses and their Application in Quantum Cascade Laser Tuning" Conference on Lasers and Electro-Optics (CLEO): CMGG6 (2007).
46. A. Zakery, and S. R. Elliot, "Optical properties and applications of chalcogenide glasses: a review," *J. Non-Cryst. Solids* **330**(1-3), 1–12 (2003).
47. K. Tanaka, "Reversible photostructural change: mechanisms, properties and applications," *J. Non-Cryst. Solids* **35–36**, 1023–1034 (1980).
48. T. T. Nang, M. Okuda, and T. Matsushita, "Photo-induced absorption change in some Se-based glass alloy systems," *Phys. Rev. B* **19**(2), 947–955 (1979).
49. N. Hô, M. C. Phillips, H. Qiao, P. J. Allen, K. Krishnaswami, B. J. Riley, T. L. Myers, and N. C. Anheier, Jr., "Single-mode low-loss chalcogenide glass waveguides for the mid-infrared," *Opt. Lett.* **31**(12), 1860–1862 (2006).
50. A. Salimonia, A. Villeneuve, T. V. Galstyan, S. LaRochelle, and K. Richardson, "First- and Second-Order Bragg Gratings in Single-Mode Planar Waveguides of Chalcogenide Glasses," *J. Lightwave Technol.* **17**(5), 837–842 (1999).
51. S. Tomljenovic-Hanic, M. J. Steel, C. Martijn de Sterke, and D. J. Moss, "High-Q cavities in photosensitive photonic crystals," *Opt. Lett.* **32**(5), 542–544 (2007).
52. Y. Yanagase, S. Yamagata, and Y. Kokubun, "Wavelength tunable polymer microring resonator filter with 9.4 nm tuning range," *Electron. Lett.* **39**(12), 922–924 (2003).
53. A. Melloni, F. Morichetti, C. Ferrari, and M. Martinelli, "Continuously tunable 1 byte delay in coupled-resonator optical waveguides," *Opt. Lett.* **33**(20), 2389–2391 (2008).
54. W. De Cort, J. Beeckman, R. James, F. A. Fernández, R. Baets, and K. Neyts, "Tuning of silicon-on-insulator ring resonators with liquid crystal cladding using the longitudinal field component," *Opt. Lett.* **34**(13), 2054–2056 (2009).
55. U. Levy, K. Campbell, A. Groisman, S. Mookherjee, and Y. Fainman, "On-chip microfluidic tuning of an optical microring resonator," *Appl. Phys. Lett.* **88**(11), 111107 (2006).
56. R. T. Brown, "Laser-assisted selective chemical etching for active trimming of GaAs waveguide devices," *IEEE Photon. Technol. Lett.* **2**(5), 346–348 (1990).
57. M.-C. M. Lee, and M. C. Wu, "Tunable coupling regimes of silicon microdisk resonators using MEMS actuators," *Opt. Express* **14**(11), 4703–4712 (2006).
58. F. Xia, M. Rooks, L. Sekaric, and Y. Vlasov, "Ultra-compact high order ring resonator filters using submicron silicon photonic wires for on-chip optical interconnects," *Opt. Express* **15**(19), 11934–11941 (2007).
59. B. E. Little, S. T. Chu, H. A. Haus, J. Foresi, and J.-P. Laine, "Microring resonator channel dropping filters," *J. Lightwave Technol.* **15**(6), 998–1005 (1997).
60. A. Melloni, and M. Martinelli, "Synthesis of Direct-Coupled-Resonators Bandpass Filters for WDM Systems," *J. Lightwave Technol.* **20**(2), 296–303 (2002).
61. T. Sudoh, Y. Nakano, and K. Tada, "Wavelength trimming technology for multiple-wavelength distributed feedback laser array by photo-induced refractive index change," *Electron. Lett.* **33**(3), 216–217 (1997).
62. M. W. Lee, C. Grillet, C. L. Smith, D. J. Moss, B. J. Eggleton, D. Freeman, B. Luther-Davies, S. Madden, A. Rode, Y. Ruan, and Y. H. Lee, "Photosensitive post tuning of chalcogenide photonic crystal waveguides," *Opt. Express* **15**(3), 1277–1285 (2007).

1. Introduction

Chalcogenide glasses (ChGs) are well-known for their high infrared transparency and amenability to fabrication in fiber and thin film forms which makes them attractive candidates for mid-IR optical chemical sensors. However, they are also well-known for a variety of properties which can complicate the utility of these materials in traditional applications, including low thermal stability, low chemical durability and photosensitivity, as compared to oxide materials. Traditional fabrication techniques such as thermal evaporation and photolithography have been shown to be viable for large-scale production of planar optical devices, but can suffer from drawbacks, such as poor compositional fidelity and high post-fabrication surface roughness which can lead to increased optical loss. Such attributes can adversely affect the detection limit and sensitivity of the final sensor system.

In this paper we will present several methods for using these material properties in order to overcome such challenges in the fabrication of planar optical resonator systems, and their application as sensors. The low glass transition temperature (T_g) has been utilized in applying

thermal reflow techniques to reduce optical loss. The solubility of these glasses in alkaline environments has been harnessed to create spin-on cladding layers with excellent compositional fidelity for optical loss reduction. Such processing flexibility opens-up novel fabrication techniques, including capillary force lithography that allows the creation of waveguide and grating structures in a single step. The intrinsic photosensitivity of the ChG materials has been utilized to fine-tune the effective refractive index of ChG waveguides, and thereby the resonant wavelength of micro-ring resonators. By using such trimming techniques, a local post-fabrication “repair” of photonic devices has been demonstrated. This process flexibility reduces component cost and enhances device performance, otherwise not possible. Discussed in this paper are the details of such capabilities and how these “traditionally” considered material limitations can be used to the advantage of device designers and fabricators creating novel functional components from ChGs.

2. Material engineering for low-loss photonic device processing

2.1 Optical loss reduction: the key to highly sensitive chem-bio detection

Optical loss reduction has been a recurring theme and device performance necessity for the systems used for sensing mechanisms currently under investigation including, Refractometry Sensing (RS) of surface molecular binding, as well as Cavity-Enhanced Absorption Spectroscopy (CEAS) and Micro-Cavity Photo-Thermal Spectroscopy (MC-PTS) for infrared molecular absorption detection. Phenomenologically, low optical loss suggests a long, resonantly-enhanced optical path length in the resonant cavity device, which in turns creates strong photon-molecular interaction. Such enhanced interaction manifests itself as high cavity quality factors (Q-factor) and leads to high detection sensitivity. Quantitative analysis into the former two sensing mechanisms (RS and CEAS) has revealed that low *overall* optical loss (~0.1 dB/cm) is the key to high detection sensitivity up to a point where temperature fluctuation noise starts to take over [1,2]. In contrast, sensor optimization theory for MC-PTS suggests that the major sensor performance limitation originates from *material absorption* loss rather than scattering loss [3]. The intrinsic immunity of MC-PTS to scattering loss presents an important competitive advantage over CEAS, as scattering loss has been demonstrated to be the dominant loss mechanism in current High-Index-Contrast (HIC) chalcogenide glass photonic devices [4]. It has been shown that relative sensitivity enhancement of a factor of 10^4 over CEAS is possible in MC-PTS [3].

2.2 Understanding optical loss in HIC chalcogenide glass photonic waveguides

There are typically three main optical loss mechanisms in high-index-contrast waveguides: material attenuation, surface/sidewall roughness scattering, and radiative loss. Depending on its origin, material attenuation in chalcogenide glass can be categorized into intrinsic and extrinsic loss, where the former includes electronic absorption by band tail or mid-gap states (with nonlinear absorption neglected at low power), Rayleigh scattering caused by statistical density fluctuations, and phonon (bond vibrational) absorption. In the infrared wavebands of interest to spectroscopic sensing, Rayleigh scattering is negligible, given that the wavelength is much larger than the length scale of density fluctuation. Phonon absorption occurs at specific wavebands corresponding to the characteristic bond vibration frequencies. Such absorption bands in the ChG compositions are studied using Fourier Transform InfraRed (FTIR) spectroscopy [5], and can be carefully tailored and/or avoided via compositional engineering. For example, by alloying with constituents containing heavy atoms, the photon absorption peaks can be red shifted [6]. This approach has also been demonstrated by other authors to effectively extend the long-wave IR transmission bands [7]. Hence, the major material loss contributors are electronic absorption and extrinsic loss due to impurity absorption. Mid-gap state absorption does play a key role in the photosensitivity process of As_2S_3 chalcogenide glass at 1550 nm telecommunication wavelength [8]. It is expected, however, that mid-gap state density in glasses at these wavelengths may be controlled to yield low optical loss through selective addition of certain chemical modifiers, reducing the length

of the Urbach tail. The validity of this approach has been verified by a number of groups [9,10], although detailed mechanistic studies are required to completely clarify the underlying physics of such chemical modification. Alternately, the composition may be modified in order to increase the optical band gap; however, this will also potentially influence thermal properties, and the photo-response of the glass, the impact of which must also be considered.

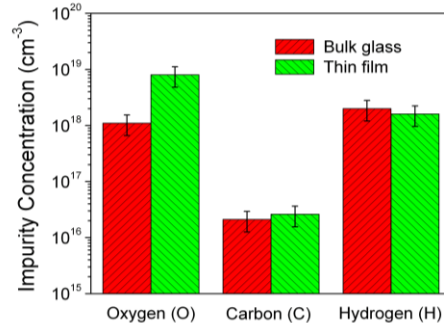


Fig. 1. Oxygen, carbon and hydrogen impurity concentrations in bulk $\text{Ge}_{23}\text{Sb}_7\text{S}_{70}$ glass and thin films thermally evaporated from the same batch of bulk glass.

As for extrinsic loss, while impurity-induced optical loss has been relatively well examined in chalcogenide optical fibers [11–13], studies into impurities and associate optical loss in planar chalcogenide glass thin films have to date, been scarce. Towards this end, preliminary studies have been performed to ascertain the impact of thin film processing on impurity incorporation. Figure 1 shows oxygen, carbon and hydrogen impurity concentrations in bulk $\text{Ge}_{23}\text{Sb}_7\text{S}_{70}$ glass and thin films deposited from the same batch of bulk glass, measured using Secondary Ion Mass Spectroscopy (SIMS). The bulk glass has been synthesized using the traditional melt-quenching techniques and no subsequent purification has been performed. The films have been thermally evaporated onto silicon wafers and are ~500 nm in thickness [14]. The SIMS analysis reveals that the impurity concentrations remain almost constant along the thickness of the film indicating the absence of surface segregation effects. Further, it is evident that while carbon and hydrogen concentrations remain identical between films and bulk, oxygen concentration in thin films are increased by almost 7-fold as compared to bulk, suggesting that residual oxygen in the high-vacuum (3×10^{-7} Torr) chamber has been incorporated into the film during deposition. Carbon and hydrogen have been shown to be successfully removed via purification of elemental starting materials [15,16]. Similar trends have been observed in As_2S_3 chalcogenide glass bulk and films. The increase of oxygen impurity concentration in thin films may have a significant impact on planar photonic device loss: it is expected that the optical loss in the O-H absorption band (centered around 2.9 μm) is correspondingly increased compared to the loss in bulk, a factor to be taken into account when designing sensor devices operating at these wavelengths. The fact that little new C and H impurities are introduced into the films also suggest a practical method for thin film optical loss reduction in the respective absorption bands simply by starting with purified glass materials for deposition.

Roughness scattering arising from imperfections on device surfaces is particularly severe in HIC waveguiding systems, since the scattering loss scales with refractive index difference [17]. In particular, most scattering loss is associated with scattering from sidewall roughness, as the top surface of devices are usually formed during an additive deposition process and generally feature small RMS roughness. In contrast, plasma etch patterning is conventionally employed for planar device fabrication; consequently, the sidewalls are formed during a subtractive etching process, which can lead to excessive roughness and hence increased optical loss [18].

Radiative loss refers to optical loss due to coupling into radiative or substrate modes caused by waveguide bending or quantum tunneling through a finite cladding thickness.

Radiative loss is suppressed in our devices simply by proper device geometry design. The experimentally measured waveguide loss values usually represent the arithmetic sum of all these loss sources, and thus special techniques need to be employed to identify the individual contributions from each of these mechanisms [18–22]. In HIC strip waveguides made of Ge-Sb-S glass, shallow rib waveguides have been used to measure the intrinsic material loss, as shallow rib waveguides are known to be less sensitive to sidewall roughness scattering [20]. Very low optical loss, down to 0.5 dB/cm at 1550 nm wavelength, is measured in the shallow rib waveguides made of Ge-Sb-S chalcogenide glass. In comparison, single-mode strip waveguides (750 nm wide and 400 nm high) made of the same glass composition have propagation loss numbers of (3.9 ± 0.4) dB/cm for the TM polarization and (6.4 ± 0.8) dB/cm for the TE polarization [4]. The much higher optical loss in the strip waveguides is attributed to scattering due to sidewall roughness. Atomic Force Microscopy (AFM) measurements also confirm the presence of significant sidewall roughness (RMS amplitude ~ 10 nm) on these as-fabricated waveguides, which is consistent with the loss figures measured. This study concludes that sidewall roughness scattering accounts for $> 80\%$ of optical loss in these sub-micron strip waveguides where the optical mode is tightly-confined. Similar trends, showing the increased impact of sidewall roughness on optical loss in small cross-section chalcogenide glass waveguides has been discovered and discussed by other researchers as well [23,24], which further validates the major contribution of roughness scattering to optical loss in high-index-contrast chalcogenide glass waveguides. This conclusion, therefore, highlights the critical importance of roughness scattering loss reduction. Two techniques for reducing the scattering loss mechanism, thermal reflow and a novel solution-based spin-on over layer coating method, will be discussed in the following sections.

2.3 Roughness scattering loss suppression in chalcogenide glass waveguides via thermal reflow

Viscosity in glassy materials often exhibits thermally activated behavior which may be phenomenologically described by a modified Arrhenius equation [25]. The strong dependence of viscosity on temperature leads to a dramatic reduction of the glass viscosity when the glassy materials are heated to temperatures well above their glass transition temperatures (T_g). At such temperatures, the action of surface tension leads to smoothing of roughness and thus the reduction of scattering loss due to sidewall roughness. As is shown in Fig. 2, surface tension on an undulated surface leads to high positive internal pressure in the crest and negative pressure in the trough. Such a pressure gradient creates viscous flow which accounts for the roughness reduction. This process forms the cornerstone of the thermal reflow technique. Thermal reflow has already been employed to reduce optical loss in silica photonic devices [26,27]. Applying thermal reflow to chalcogenide glasses presents several key competitive advantages over their silica counterparts: 1) the much higher refractive index of chalcogenides dictates a more significant loss reduction effect; 2) the low T_g and hence low softening temperature of chalcogenides suggest that the reflow process can be conducted at much lower temperature compared to silica, which facilitates process integration with other on-chip electronic and photonic devices; and 3) chalcogenide glasses span a vast thermal property space by composition alloying, which enables selective reflow of certain layers/patterns in complex structures (e.g. selective reflow of the waveguide core while maintaining the cladding structure intact). However, a recurring question needs to be addressed before the technique can be also successfully applied to chalcogenide glasses: does the heat treatment process (thermal reflow) induce excessive crystallization or composition segregation or volatilization (and associated optical scattering at grain boundaries or precipitates) which defeat the purpose of loss reduction?

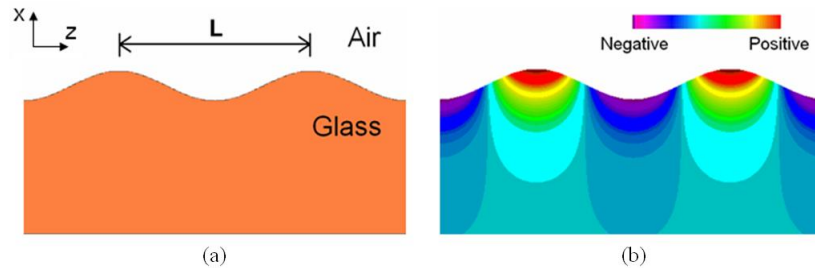


Fig. 2. (a) Schematic illustration of a glass surface with sinusoidal roughness characterized by a spatial period L ; (b) calculated internal pressure due to surface tension in glass with a rough surface (reproduced from Ref. 28).

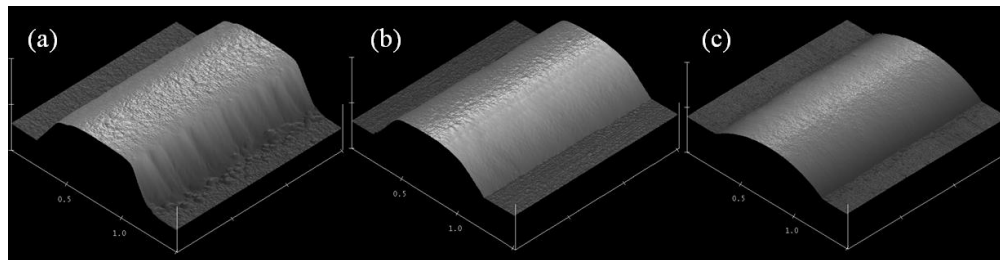


Fig. 3. Surface morphology of As_2S_3 chalcogenide waveguides measured by AFM: (a) as-patterned; (b) reflowed at 230 °C for 15 s exhibiting reduced sidewall roughness; and (c) reflowed at 245 °C for 15 s showing significant cross-sectional geometry modification (reproduced from Ref. 28).

To better understand the crystallization behavior, a direct analogy is drawn between the thermal reflow process and the optical fiber drawing process, as both processes involve heat treatment of a glass melt at temperatures well above T_g . A thermal reflow kinetic theory has been developed [28] and shows that assuming the reflow process is performed within the fiber drawing viscosity window (10^3 to 10^6 Pa·s) [14], the time it takes to reduce the roughness with a characteristic wavelength of 1 μm is approximately 10^{-3} to 0.1 s. Thus the time scale for thermal reflow is much shorter than the dwelling time of a fiber pre-form in the fiber drawing furnace. Since state-of-the-art chalcogenide glass fibers can achieve very low optical loss (< 1 dB/m) near the 1550 nm wavelength [29], this indicates that the potential precipitation of crystallites leading to optical scattering loss can be suppressed in the fiber drawing thermal process. Thus this analogy suggests that it is possible to achieve low loss chalcogenide waveguides via thermal reflow without compromising the glass material quality, given the short reflow time required and hence low crystallization tendency. However, it is worth pointing out that this analogy has neglected surface-induced crystallization effects: in thin films, the tendency to crystallize can be enhanced by the presence of a large surface-to-volume ratio [30], which can only be experimentally measured and empirically corrected as the surface crystallization rate is very difficult to model.

Experimental characterization has been performed on post-reflow-treatment planar As_2S_3 films and waveguide devices. This glass composition was selected for its superior stability against crystallization compared to the Ge-Sb-S glass system [31]. No distinctive crystallization peaks are identified on the X-Ray Diffraction (XRD) spectra for reflowed films. Given the resolution of the XRD instruments used in this experiment, one may conclude that the crystalline precipitates in the reflow films are either very small in size (< 10 nm) or that they only occupy a small volume fraction ($< 10\%$) in the glass matrix. The impact of such nanoscale crystalline precipitates on optical waveguide loss may then be semi-quantitatively modeled using the Rayleigh scattering theory. Taking the limiting case of 10 nm size crystallites occupying 10% volume fraction, the theory predicts a crystallite scattering loss upper limit of 0.7 dB/cm. Experimentally, optical loss reduction from ~ 7

dB/cm to ~ 3 dB/cm has been achieved for TE polarized light at the 1550 nm wavelength [28]; therefore, the crystallite scattering is not a major limiting factor for loss reduction in the current devices. Consequently, radiative loss has been identified to be the main loss contributor, which is attributed to the partial evaporation of As_2S_3 glass during reflow (Fig. 3). Future work thus involves starting with as-fabricated waveguides of larger cross-sectional area to compensate for the partial evaporation effect and/or compositional modification based on detailed mass spectroscopy studies which can highlight optimal thermal stability of candidate glasses. The measurements are currently in progress.

3. Solution processing as an alternate fabrication route

3.1 Waveguide over-cladding for low-temperature roughness reduction

Reduction of waveguide surface roughness can result in significant improvements in optical loss. It is also known that while the As-S glass system is relatively stable to surface crystallization during heat treatment above its T_g , some glass systems, such as Ge-Sb-S are less suitable for such processing routes [31]. It is therefore desirable to investigate alternate processing routes for obtaining low roughness surfaces at lower temperatures. It has been demonstrated that the Ge-Sb-S and As-S glass systems are soluble in basic organic solvents (amines) and are amenable to solution processing. Moreover, spin-coated films derived from these solutions were found to reach their maximum refractive index and density through sub- T_g heat treatments, making this method promising for loss reduction in glass systems with low thermal stability. To this end, a well-known solution casting method has been investigated for a novel deposition approach for thin chalcogenide layers over lithographically defined resonator systems.

Waveguides and resonators of the glass composition $\text{Ge}_{21}\text{Sb}_{11}\text{S}_{68}$ with 400 nm thickness were formed by thermal evaporation and lift-off lithography. Over-cladding layers were then deposited over these structures by spin-coating; the solution consisted of ground bulk glass which was first dissolved in propylamine for 48 hours at a concentration of 25 mg/ml. The optimized spin-coating conditions have been previously published [32], and the spin speed was chosen to give a coating thickness of 100 or 200 nm (spun at 9000 and 6000 rpm respectively). Films were heat treated under vacuum (~ 1 Torr) at varying temperatures from 120 to 180 °C for one hour. Figure 4 displays SEM micrographs of waveguides before and after solution cladding.

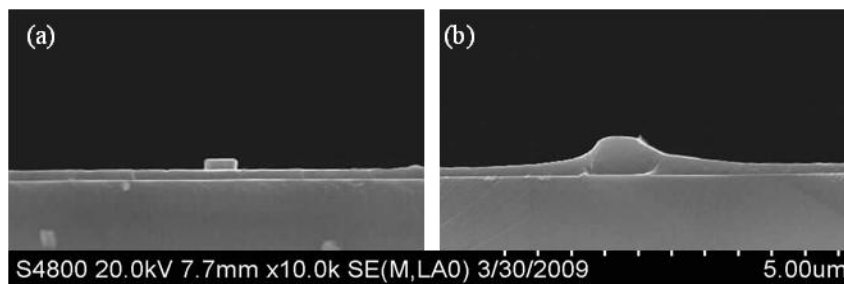


Fig. 4. Cross-sectional SEM micrograph of Ge-Sb-S waveguides (a) before and (b) after solution cladding.

It is clear that the waveguide has become thicker and wider after coating, and the profile has changed, becoming more rounded and with sloping sidewalls, as compared to the vertical sidewalls of the as-fabricated waveguide. This increased size is expected to alter the mode profile of the guide, but may be compensated for in the design of the uncoated structures. The low contrast visible in the image between the core and cladding suggest good agreement in composition, and indeed the composition of the coating was found to match that of the parent bulk glass to within ± 2 atomic percent, using energy dispersive X-Ray spectroscopy. XRD data confirms that the coating is amorphous. In order to examine the effect of coating on

surface roughness, atomic force microscopy (AFM) was performed on coated and uncoated guides. Figure 5 demonstrates single line scans along the sidewalls of the guides.

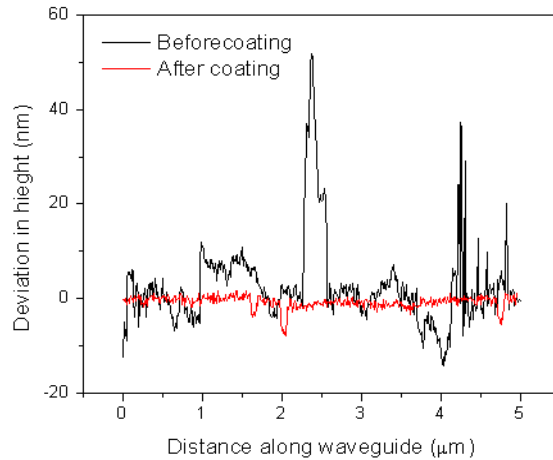


Fig. 5. AFM line scans for coated and uncoated waveguides.

The reduction in roughness is clear from the AFM results. The large number of peaks and valleys up to 50 nm in height in the uncoated waveguide have been reduced to only a few ~5 nm valleys after coating. These remaining valleys were later found to correspond to small pores in the surface of the spin-coated layer. Average RMS sidewall roughness was found to decrease from $19 (\pm 1)$ to $1.4 (\pm 0.1)$ nm due to application of the cladding layer.

Finally, the optical loss of the coated and uncoated samples at a wavelength of 1550 nm was examined. Relative loss values for guides coated at varying speeds, and heat treated at various temperature are shown in Fig. 6.

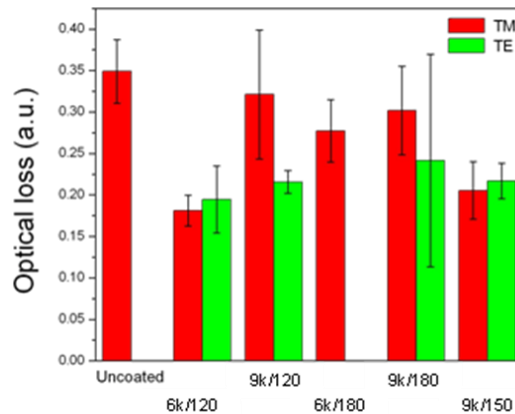


Fig. 6. Relative optical loss at 1550 nm for coated waveguides as a function of spin-speed and hard-bake temperature (speed/temperature).

It is clear that solution over-cladding can be used to reduce the optical loss of lithographically defined planar ChG waveguides. It is interesting to note that the loss systematically increases if the thickness of the coating is decreased, or the heat treatment temperature is increased, despite similar roughness values for all coated guides. Because the refractive index of solution-derived films has been shown to increase with higher heat treatment temperatures, this suggests that there are two mechanisms for the loss reduction. The first mechanism is through roughness reduction, while the second is through the increase of waveguide cross-sectional dimensions and hence reduced optical mode overlap with the

sidewalls. It is also interesting to note that the TE polarization exhibits lower loss than the TM polarization in the coated waveguides. As the TE mode in HIC waveguides is typically far more susceptible to roughness scattering than the TM counterpart, the experimental observation suggests that sidewall roughness scattering is becoming insignificant in the overall loss contribution. Design of an optimized overlayer coating thickness and heat treatment procedures may lead to application of this technique with improved loss values compared to those found in this non-optimized study, which is promising for future low-loss IR photonics applications.

3.2 Direct fabrication of waveguides using solution-based methods

It has been recently demonstrated that ChG waveguides can be fabricated directly using solution-based methods [33], which has the potential to simplify processing of devices. Unfortunately, the existing capillary flow technique [33] does not allow the fabrication of isolated structures such as disk and ring resonators, which have proven to be critical for achieving low detection limits and high sensitivity in planar optical sensor platforms [1–4]. Alternative methods, such as ink-jet printing [34] and micro-contact printing [35] may have the potential to fabricate such geometries, but printing techniques do not currently allow sufficient pattern fidelity to achieve low-loss structures, and all of the above techniques suffer from the need for good wetting of the glass solution to the mold and substrate materials, limiting the choice of the solution chemistry [33]. Proposed here is an alternate soft-lithography [36] technique that may remedy these drawbacks, known as capillary force lithography (CFL) [37], which is illustrated in Fig. 7.

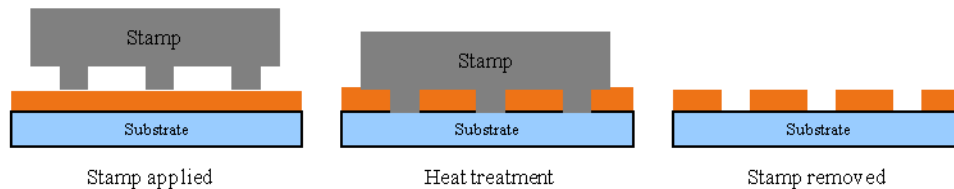


Fig. 7. Process flow chart for capillary force lithography technique.

In this technique, a thin film is first formed by spin-coating onto a glass or semiconductor substrate. A PDMS mold is then applied to the surface of the film, and the system is exposed to elevated temperatures in order to allow viscous flow. When the mold is removed from the film at room temperature, the inverse of the pattern in the mold is retained in the film. This is similar to commonly used embossing methods, wherein a mold is pressed against the surface of the film and increased temperature is used to allow the film to flow. In this case however, the mold is applied to the surface during the natural heat treatment process used to remove solvent from the solution-derived film after spin-coating [32], preventing the use of additional high-temperature processing steps and avoiding potential thermal stability concerns.

As a proof of concept, a grating has been prepared by first casting a PDMS stamp on the surface of a standard re-writable compact disk (CDRW). This created a mold with a sinusoidal grating pattern with a 200 nm line height and 2 μm pitch. The mold was then applied to a 500 nm thick As_2S_3 film which was heated to near its T_g (210 $^\circ\text{C}$) and held for a period of 30 minutes before being cooled to room temperature. Figure 8 presents AFM surface profiles of the resulting grating.

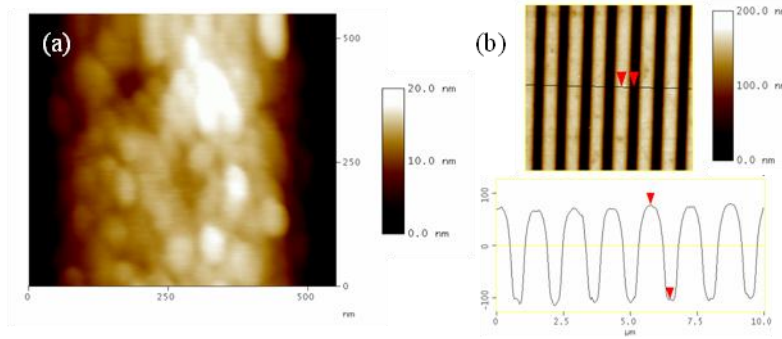


Fig. 8. High (a) and low (b) resolution scans of CFL-derived As_2S_3 grating, showing good reproduction of mold geometry, but with high roughness.

It was found that CFL gratings formed in As_2S_3 near T_g show relatively high surface roughness, which has been attributed to phase separation and crystallization of realgar (As_4S_4) from the film (confirmed using XRD). In order to demonstrate the utility of solution-based fabrication for decreased surface roughness, the same procedure was repeated for solution-derived films, and the mold was applied either during the initial soft-bake (1 hr at 90°C under N_2) or during the hard-bake (1 hr 150°C under vacuum) heat treatment. AFM surface scans for low-temperature CFL gratings are shown in Fig. 9.

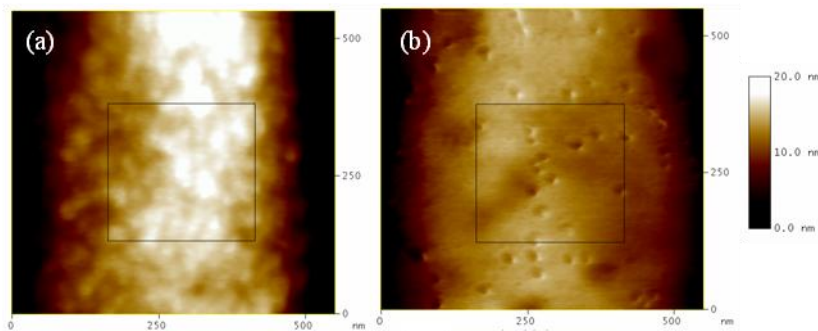


Fig. 9. AFM surface profiles for soft-bake (a) and hard-bake (b) CFL-derived As_2S_3 grating, showing significantly improved surface roughness.

From the figure, it is clear that the surfaces of the low-temperature CFL gratings are significantly less rough. RMS surface roughness was found to decrease from 23 nm with CFL at 210°C to 1.3 and 0.9 nm when CFL was performed on solution-derived films at 90°C and 150°C respectively. The occurrence of viscous flow at temperatures well below the T_g of the corresponding bulk glass suggests that residual solvent molecules present in the film depolymerize the glass network, leading to lower viscosity at a given temperature. The fact that the mold surface is precisely duplicated even at such low temperatures demonstrates the potential of capillary force lithography for the direct fabrication of low-roughness ChG planar devices even for low-stability compositions. Because many devices can be created from each mold, and many PDMS molds from each master, there is great potential for large-scale and rapid fabrication of complete devices. It should also be noted that these patterns covered relatively large areas (25 mm diameter) and the solvent evaporation was found to be equally complete at the center and edge of the grating, suggesting that solvent evaporates through the PDMS mold by diffusion, rather than along the grating lines. This observation supports the idea that this technique is not limited to small gratings or waveguides. Complex geometries such as micro-lens arrays and resonators can also theoretically be reproduced over large areas, provided that the mold design can mechanically support the necessary aspect ratio, and a film

of sufficient thickness is first deposited. A complete study comparing the optical loss of lift-off waveguides and resonator systems to their CFL counterparts is currently ongoing.

4. Leveraging photosensitivity for post-fabrication trimming

High photosensitivity in the visible spectrum is a well-known and widely used property of ChGs [38–42], and solution-derived ChG films have recently been shown to exhibit photosensitivity similar to that of traditional thermally evaporated films [43–45]. The absorption of light with near-band gap energy produces local modifications of the atomic structure of the glass and therefore to its optical properties, i.e. electronic band gap and refractive index [46]. The magnitude and sign of these photoinduced changes, as well as their thermal reversibility are highly dependent on the chemical composition and the fabrication process of the specific glass as well as the exposure conditions [47,48]. The photoinduced refractive index change Δn of chalcogenide materials can be exploited to directly write optical planar waveguides [49], Bragg gratings [50] or photonic crystal cavities [51]. Besides these, the opportunity for large induced index variation (up to 4×10^{-2}) [46] using low illumination intensities as well as the flexibility and the simplicity of the principle make photosensitivity in ChG-based integrated devices a promising tool for a variety of novel applications.

For instance, in order to achieve target specifications for desired functionalities, integrated optical circuits require a high degree of accuracy, uniformity and reproducibility in the definition of the geometric and optical parameters of the waveguides. These requirements become even more challenging when resonant structures based on micro-rings, micro-disks, or photonic crystals are exploited to make compact, sensitivity-enhanced and highly selective devices for filtering and sensing applications. The capability to realize a post-fabrication permanent trimming of both the local and global properties of photonic devices is therefore highly attractive.

The irradiation of resonant structures allows tuning of the working wavelength or the optimization of its local parameters for different applications. This enables lower acceptable fabrication tolerances, by permitting post-fabrication reconfiguration of the optical components. In contrast to other previously investigated tuning and trimming techniques, such as thermo-optic effects [52,53], liquid crystal or micro-fluidic channel integration [54,55], post-process chemical treatments [56] or mechanical deformation [57], the photosensitivity approach does not require additional fabrication steps and enables local control of the refractive index over an area down to micrometer scale. Initial results regarding the tuning of an As_2S_3 resonant device made by two directly coupled micro-ring resonators are presented here.

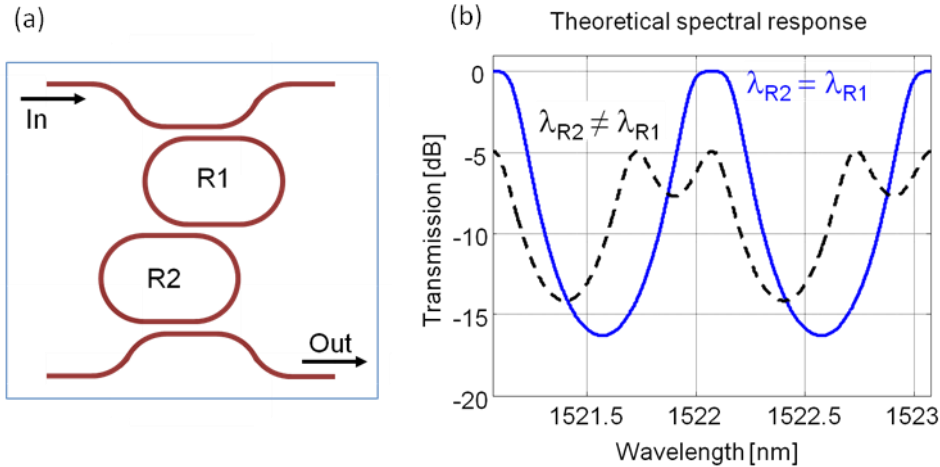


Fig. 10. (a) Schematic of a second order filter made by two directly coupled micro-ring resonators; (b) theoretical spectral response of the filter with FSR = 1 nm and B = 0.25 nm when $\lambda_{R1} = \lambda_{R2}$ (blue solid line), and when $\lambda_{R1} - \lambda_{R2} = \text{FSR}/3 = 0.3$ nm (black dashed line).

The scheme of this device, realizing a second order optical filter, is shown in Fig. 10(a). Despite its simplicity, this structure already includes the critical attributes of more complex coupled-resonator devices employed in advanced applications [58]. When the two rings have the same resonance wavelength, $\lambda_{R1} = \lambda_{R2} = \lambda_R$, i.e. when their optical length is exactly the same, an optical signal incoming from the input port (In) is transmitted to the output port (Out) only if its wavelength matches the resonance wavelength of the rings; otherwise, the input signal continues propagating in the input bus waveguide [59]. A careful design of the power coupling coefficients between the rings and between each ring and the bus waveguide allows the shaping of a flat pass-band with the desired width and extinction ratio [60]. As an example, the blue solid curve in Fig. 10(b) shows the theoretical spectral response of an ideal double-ring filter with free spectral range FSR = 1 nm and bandwidth B = 0.25 nm.

Typically $\lambda_{R1} \neq \lambda_{R2}$ due to unavoidable fabrication imperfections and the resulting spectral response is quickly distorted, strongly affecting device functionalities. The black dashed line in Fig. 10(b) shows the theoretical device spectral response for a wavelength shift $\Delta\lambda_R = \lambda_{R1} - \lambda_{R2} = 0.3$ nm, corresponding to one-third of the spectral periodicity. Deep in-band ripples, reduced transmission, bandwidth broadening and extinction ratio reduction are clearly visible phenomena.

To underscore how demanding this issue can be, it should be recalled that the relative wavelength shift $\Delta\lambda_R / \lambda_R = \Delta n / n_g = \Delta L_r / L_r$, where n_g is the group refractive index (typically $n_g = 2.48$ for As_2S_3 waveguides) and L_r is the geometrical length of the ring. A resonance wavelength error of $\Delta\lambda_R = 0.3$ nm means an error in the ring length of only $\Delta L_r = 180$ nm or, more challenging, a refractive index error of $\Delta n = 5 \times 10^{-4}$. As n_g varies with the width of the guide, this corresponds to a waveguide width error of only $\Delta w = \Delta n (\delta w / \delta n_g) \approx 2.5$ nm (as $\delta n_g / \delta w$ is typically in the order of $2 \times 10^{-4} \text{ nm}^{-1}$). This value is well below the typical technological tolerances guaranteed by the fabrication process, as discussed in Sec. 2.2.

To demonstrate the use of post fabrication trimming, two-ring As_2S_3 filters were fabricated with bending radius $R = 100 \mu\text{m}$ and coupling straight sections with a $L_c = 150 \mu\text{m}$, providing FSR = 130 GHz (corresponding to 1.04 nm); employed strip waveguides are 450 nm high and 800 nm wide, with an estimated $n_g = 2.48$ and are realized using the method described in [4]; coupling sections have all the same gap size (700 nm), while the desired coupling coefficients are obtained by shifting the rings, as shown in the photograph of Fig. 11(a).

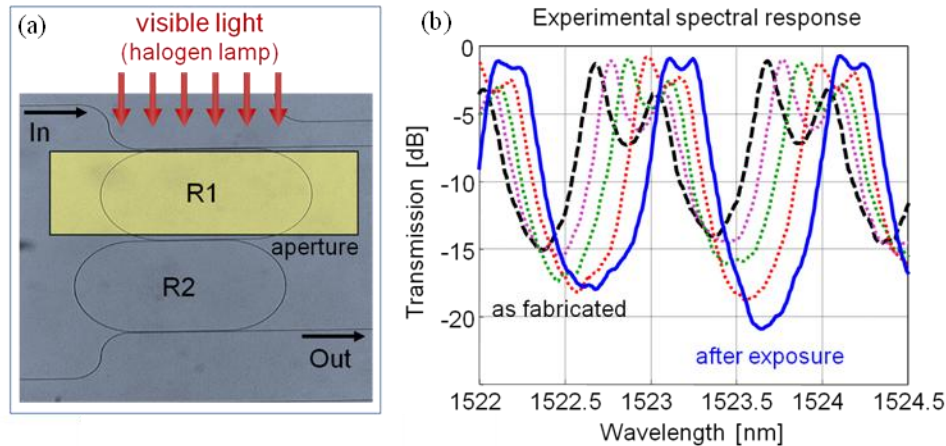


Fig. 11. (a) Photograph of the As_2S_3 two-ring device and schematic of the post-fabrication photoinduced trimming process: the sample is selectively illuminated with visible light through a rectangular aperture; (b) experimental spectral response of the filter: as fabricated (black dashed line), during the progressive tuning of resonances (dotted lines) and in the tuning condition after the exposure (blue solid line) (Media 1).

The measured spectral response of the as fabricated device, which is shown as a black dashed line in Fig. 11(b), suffers from a relative detuning of the rings' resonance wavelengths of about $\Delta\lambda_R = 0.35$ nm. Therefore, the ChG glass photosensitivity was used to tune the resonant wavelength of the rings, compensating for the fabrication inaccuracies. According to the scheme in Fig. 11(a), the ring (R1) with the lowest resonance wavelength λ_{R1} was illuminated by a halogen lamp through a rectangular aperture in a mask, while the rest of the surface of the chip was shadowed. The rectangular aperture has a minimum size of $100\ \mu\text{m}$ and was mounted on a 3-axis micro-positioning stage. In this way, selective change of the refractive index is induced in ring R1 only, in order to finely tune its resonance wavelength up to that of the other resonator. The halogen lamp has an intensity of $0.3\ \text{mW}/\text{cm}^2$, with most of the emission spectrum lying in the visible region from 450 nm to 650 nm.

The progressive red-shift of λ_{R1} from the initial condition (black dashed line) to the tuned condition $\lambda_{R2} = \lambda_{R1}$ (blue solid line) is reported in Fig. 11(b) (Media 1). After exposure, the device shows a flat pass-band with a band width of 32.5 GHz and an extinction ratio of about 20 dB, in good agreement with design specifications and the ideal response reported in Fig. 10(b). It should be noticed that the photoinduced trimming does not induce any additional observable loss, demonstrating the great potential of this approach.

Once the desired shape of the spectral response is recovered, photosensitivity can be further exploited to finely adjust the working wavelength of the device, as previously demonstrated in distributed feedback lasers [61] and in photonic crystals [62]. The control of the absolute spectral position is indeed a fundamental issue in many applications, not only in sensing, but also, for instance, in the optical communication field. To this purpose, a "rigid" spectral shift of the filter response is required. By removing the aperture and completely illuminating the device, the refractive index was simultaneously changed throughout the whole circuit. Experimental results are shown in Fig. 12(a) (Media 2). The transfer function is progressively red-shifted, in less than 4-minute exposure, from the initial position (black dashed line) over a full FSR, i.e. over 1 nm wavelength range (blue solid line), without any visible distortion or performance degradation. Moreover, after the trimming process, the spectral response remains stable in time. The device was stored in dark and measured again after one week to check the spectral drift. Experimental results shown in Fig. 12(b) demonstrate that there are no significant differences between the spectral response measured at the end of the exposing cycles (black dashed line) and one week later (blue solid line).

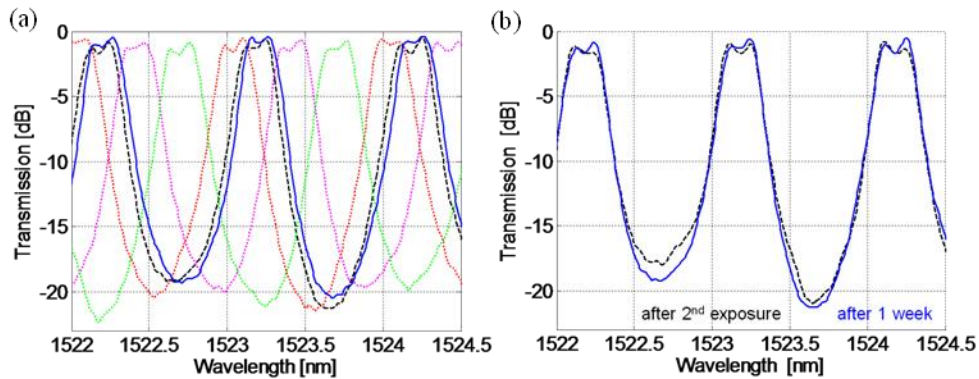


Fig. 12. (a) Permanent tuning of the device working wavelength by visible light exposure of the whole circuit: from the initial position (black dashed line), the experimental spectral response is “rigidly” shifted over a full FSR (blue solid line). (Media 2); (b) comparison between the experimental spectral responses measured immediately after the 2nd exposure (black dashed line) and after 1-week storage in dark (blue solid line).

The illumination of the whole device was then allowed to proceed over 20 FSRs, corresponding to an overall wavelength shift of 20 nm and to a variation of the waveguide effective index of 3.2×10^{-2} . Neither spectral distortions nor saturation effects were observed until that point. The trimming velocity can be easily controlled by varying the light intensity. In these experiments a maximum rate of 0.25 nm/minute was achieved with a light intensity of 2 mW/cm^2 , reducing in this way the trimming time of the devices.

5. Conclusions

This work has demonstrated several ways in which the unique properties of chalcogenide glasses, often seen a drawbacks, can be used to achieve unique applications. The low glass transition temperatures of ChGs, when combined with their high thermal stability against crystallization, allows thermal reflow of planar optical waveguides. Thermal reflow was shown to decrease residual surface roughness, and thereby optical loss. The achievement of such low loss figures is crucial to the development of high-sensitivity optical sensors.

The solubility of these materials in alkaline conditions allows for the production of IR-transparent thin films from non-aqueous amine-based solvents. The application of solution derived coatings allows for alternate route to roughness and loss reduction even in compositions that display low thermal stability. Additionally, solution processing allows for the direct fabrication of complex optical structures using capillary force lithography in a single step, without the need for high-vacuum processing. This simple and rapid technique offers the potential for rapid large-scale production.

The photosensitivity of chalcogenide glasses allows for a permanent refractive index change achieved using visible light exposure. In As_2S_3 glasses, no relaxation effect was observed within a time scale of several weeks in experimental devices. This can be usefully exploited for post-fabrication trimming of optically resonant devices for a broad range of applications, in order to compensate for local fabrication imperfections and to finely adjust the working wavelength of photonic devices enabling reduced component cost with enhanced their performance. Post-processing refinement alleviates the need for restrictively tight fabrication tolerances, and may benefit many applications in telecommunications and optical sensing.

Acknowledgments

Funding for this work has been provided (Clemson and MIT) by the US Department of Energy [Contract # DE-FG52-06NA27502] and Defense Advanced Research Projects Agency (DARPA) (MIT). The latter program is executed by the Microsystems Technology

Office (MTO) under Award No. 017535-001, ARO Award No. W911NF-09-1-0411, Program Code: A.07, Program Director: Michael Haney. The (Milano and MIT) authors acknowledge the “Progetto Roberto Rocca” (<http://web.mit.edu/progettorocca/index.html>) for partial financial support. This paper has been prepared as an account of work partially supported by an agency of the United States Government. Neither the United States Government nor any agency thereof, nor any of their employees, makes any warranty, express or implied, or assumes any legal liability or responsibility for the accuracy, completeness or usefulness of any information, apparatus, product or process disclosed, or represents that its use would not infringe privately owned rights. Reference herein to any specific commercial product, process, or service by trade name, trademark, manufacturer, or otherwise does not necessarily constitute or imply its endorsement, recommendation, or favoring by the United States Government or any agency thereof. The views and opinions of authors expressed herein do not necessarily state or reflect those of the United States Government or any agency thereof.